

Disparity-driven heterogeneous nucleation in finite-size adaptive networksAkash Yadav ¹, Jan Fialkowski,^{2,3} Rico Berner ⁴, V. K. Chandrasekar,^{5,*} and D. V. Senthilkumar ^{1,†}¹*School of Physics, Indian Institute of Science Education and Research, Thiruvananthapuram-695551, Kerala, India*²*Complexity Science Hub Vienna, Josefstädter Straße 39, 1080 Vienna, Austria*³*Center for Medical Data Science, Medical University Vienna, Spitalgasse 23, 1090 Vienna, Austria*⁴*Department of Physics, Humboldt-Universität zu Berlin, Newtonstraße 15, 12489 Berlin, Germany*⁵*Centre for Nonlinear Science & Engineering, School of Electrical & Electronics Engineering, SASTRA Deemed University, Thanjavur-613401, Tamil Nadu, India*

(Received 27 January 2024; accepted 16 April 2024; published 14 May 2024)

Phase transitions are crucial in shaping the collective dynamics of a broad spectrum of natural systems across disciplines. Here, we report two distinct heterogeneous nucleation facilitating single step and multistep phase transitions to global synchronization in a finite-size adaptive network due to the trade off between time scale adaptation and coupling strength disparities. Specifically, small intracluster nucleations coalesce either at the population interface or within the populations resulting in the two distinct phase transitions depending on the degree of the disparities. We find that the coupling strength disparity largely controls the nature of phase transition in the phase diagram irrespective of the adaptation disparity. We provide a mesoscopic description for the cluster dynamics using the collective coordinates approach that brilliantly captures the multicluster dynamics among the populations leading to distinct phase transitions. Further, we also deduce the upper bound for the coupling strength for the existence of two intraclusters explicitly in terms of adaptation and coupling strength disparities. These insights may have implications across domains ranging from neurological disorders to segregation dynamics in social networks.

DOI: [10.1103/PhysRevE.109.L052301](https://doi.org/10.1103/PhysRevE.109.L052301)

Introduction. Complex systems [1–3], characterized by their intricate interconnections, often exhibit transitions from incoherence to coherence [4–6]. Phase transitions are observed in several physical phenomena including crystallization and ferromagnetic transition. Beyond the physical systems, phase transitions in complex networks can shed more light on intriguing biological, ecological, and social problems such as population collapse and species extinction [7], polarization in society [8], and crashes in financial markets [9]. Particularly, transitions from incoherence to synchronization have been extensively studied employing various network topologies of real-world relevance [10–12]. Traditionally, most studies have been primarily concentrated on static networks. However, a large class of real-world networks coevolve with their dynamical states and adapt to the prevailing environments. For instance, from intricate dynamics of human brain [13–15], technological systems [16–18], and biological networks [19–21] to social dynamics [22–24], adaptability manifests in the entire spectrum of complex networks across disciplines.

Recent interest in adaptive dynamical networks has surged due to their potential in addressing complex systems [25,26]. Adaptively coupled phase oscillator models are paradigms for describing the interplay of function and structure in complex systems [27]. Dynamical features such as frequency clusters

[28,29], solitary states [30], recurrent synchronization [31], and heterogeneous nucleation [32] are specific to adaptive dynamical networks [33]. In addition to adaptivity, large-scale systems consist of multiple populations exhibiting diverse and multiscale behavior [34–36]. Examples include dynamics of distinct brain regions spanning multiple time scales [37], ecological communities exhibiting different time scales in response to infectious diseases [38–40], and time scales of social ties formation also vary across communities [41,42]. These investigations also reveal that time scale disparity plays a nontrivial role in shaping their collective dynamics. Studies have shown that depending on various factors, a system may opt for different routes during phase transition. For instance, multiple nucleation pathways can unfold in crystal formation, each involving distinct intermediate states [43,44]. Similarly, in the opinion formation dynamics on social networks, individuals can form a cohesive community with consensus or can form fragmented structures known as echo chambers [45,46]. The ability to manipulate the transition pathways holds immense importance as it allows to steer the system through the appropriate intermediate states under favorable conditions.

In this work, we consider a finite-size adaptive network comprised of two populations with time scale adaptation disparity and coupling strength disparity without any quenched disorder. We observe two distinct nucleation. In the first scenario, we find a single large interpopulation frequency cluster emerges at the population interface due to the coalescence of small intrapopulation clusters. The single large interfrequency cluster eventually enlarges to the system size

*chandru25nld@gmail.com

†skumar@iisertvm.ac.in

as a function of the coupling strength facilitating a multi-step transition to global synchronization. In sharp contrast, intrapopulation clusters nucleate and coalesce together to manifest two completely entrained intrapopulation clusters as a function of the coupling strength for a strong intrapopulation adaptation rate. Finally, the two intraclasses merge together for a large coupling strength resulting in a single-step transition to synchronization. Recently, similar heterogeneous nucleation resulting in multistep and single-step transitions are reported to be facilitated only by the presence of distinct disorders [32] in a single population. However, here we show the manifestation of similar heterogeneous nucleation leading to distinct phase transitions solely due to adaptation and coupling strength disparities among two populations. A strong interpopulation coupling strength always favors nucleation of interfrequency clusters leading to multi-step transition even with a strong intrapopulation adaptation rate. Similarly, a strong intrapopulation coupling strength always favors nucleation of intrafrequency clusters facilitating single-step transition even with a strong interpopulation adaptation rate. These results reveal that the disparity in the coupling strength determines the nature of nucleation leading to distinct synchronization transition. We analytically deduce the macroscopic evolution equations for the cluster dynamics using the collective coordinates framework [47] and show that the latter corroborates the simulation results. Further, we also deduce the upper bound for the coupling strength for the existence of two intraclasses explicitly, at which the abrupt single-step transition manifests, in terms of adaptation and coupling strength disparity parameters.

The model. We consider an extension to the adaptive Kuramoto model, which has been used as a paradigmatic model to study synchronization phenomena in fields ranging from neuronal networks to electrical circuits [48]. Our model comprises of N globally coupled phase oscillators with adaptive coupling represented as

$$\frac{d\phi_i^\eta}{dt} = \omega_i^\eta - \frac{1}{N} \sum_{\eta'} \sigma_{\eta\eta'} \sum_{j=1}^{N_{\eta'}} \kappa_{ij}^{\eta\eta'} \sin(\phi_i^\eta - \phi_j^{\eta'}), \quad (1a)$$

$$\frac{d\kappa_{ij}^{\eta\eta'}}{dt} = -\varepsilon_{\eta\eta'} [\kappa_{ij}^{\eta\eta'} + \sin(\phi_i^\eta - \phi_j^{\eta'} + \beta)], \quad (1b)$$

where ω_i^η and $\phi_i^\eta(t)$ are the natural frequency and the phase of the i th oscillator ($i = 1, 2, \dots, N_\eta$) in the η th population, respectively. Here, we consider two equally sized populations $\eta = \{A, B\}$. The coupling weights $\kappa_{ij}^{\eta\eta'}(t) \in [-1, 1]$ coevolve with the phases of the oscillators, $\sigma_{\eta\eta'}$ is the coupling strength, $\varepsilon_{\eta\eta'}$ is the time-scale parameter determining the adaptation rate of the coupling weights, and the parameter β accounts for different adaptation rules [49,50]. We have fixed $\beta = -0.53\pi$, close to the symmetric rule [32], which is also referred to as Hebbian adaptation rule.

Interpopulation and intrapopulation coupling strengths are governed by $\sigma_{AA} = \sigma(1 + \Lambda_\sigma)$ and $\sigma_{AB} = \sigma(1 - \Lambda_\sigma)$, respectively, where Λ_σ is the coupling strength disparity parameter, and σ is the control parameter. Analogously, interpopulation and intrapopulation time scales are governed by $\varepsilon_{AA} = \varepsilon(1 + \Lambda_\varepsilon)$ and $\varepsilon_{AB} = \varepsilon(1 - \Lambda_\varepsilon)$, respectively, where Λ_ε is the adaptation disparity parameter. When $\Lambda_\sigma = \Lambda_\varepsilon = 0$,

the network reduces to a single homogeneous population without any disparity as in [32]. $\sigma_{AA}(\sigma_{AB})$ and $\varepsilon_{AA}(\varepsilon_{AB})$ are larger (smaller) for $\Lambda_\sigma > 0$ and $\Lambda_\varepsilon > 0$, and smaller (larger) for $\Lambda_\sigma < 0$ and $\Lambda_\varepsilon < 0$, respectively. The interactions are chosen to be symmetric with $\sigma_{AA} = \sigma_{BB}$, $\varepsilon_{AA} = \varepsilon_{BB}$, $\sigma_{AB} = \sigma_{BA}$, and $\varepsilon_{AB} = \varepsilon_{BA}$. Note that rescaling of time t with the transformations $\omega_i \rightarrow \omega_i'/\tau$, $\sigma \rightarrow \sigma'/\tau$, and $\varepsilon \rightarrow \varepsilon'/\tau$ retains the dynamics of the model, where τ is a constant factor.

Results. The system of $N = 50$ adaptively coupled phase oscillators (1) are numerically solved using the Runge-Kutta fourth order integration scheme. We assign oscillators with indices $i = 1, \dots, N/2$ to the first population, and oscillators with indices $N/2 + 1, \dots, N$ are assigned to the second population. The oscillators in each population are sorted in the increasing order of their natural frequencies. ϕ_i^η 's are chosen randomly from the interval $[0, 2\pi)$. We have fixed $\kappa_{ij}^{\eta\eta'}(0) = 0 \forall i, j, \varepsilon = 0.01$, and $\beta = -0.53\pi$.

We employ the synchronization index S [32], to quantify the degree of coherence in the network, represented as

$$S = \frac{1}{N^2} \sum_{\eta, \eta'} \sum_{i=1}^{N_\eta} \sum_{j=1}^{N_{\eta'}} s_{ij}^{\eta\eta'}, \quad (2)$$

where $s_{ij}^{\eta\eta'}$ measures the pairwise frequency synchronization between i th and j th oscillators defined as

$$s_{ij}^{\eta\eta'} = \begin{cases} 1, & \text{if } |\langle \dot{\phi}_i^\eta \rangle - \langle \dot{\phi}_j^{\eta'} \rangle| \leq \delta, \\ 0, & \text{if } |\langle \dot{\phi}_i^\eta \rangle - \langle \dot{\phi}_j^{\eta'} \rangle| > \delta, \end{cases} \quad (3)$$

where δ is a predefined threshold and $\langle \dot{\phi}_i^\eta \rangle = \lim_{T \rightarrow \infty} (1/T) \int_{T_0}^{T_0+T} \dot{\phi}_i^\eta dt$ is the mean phase velocity of the i th oscillator calculated after a large transient T_0 . For $S = 1$, the system is completely synchronized, whereas $S = 1/N$ corresponds to complete incoherence.

First, we discuss the phase transition facilitated solely by the adaptation disparity Λ_ε when $\Lambda_\sigma = 0$. The network (1) exhibits a multistep transition to global synchronization as a function of σ for $\Lambda_\varepsilon = -0.5$ as depicted in Fig. 1 (green/light gray squares). The dynamics of the coupling weights $\kappa_{ij}^{AB}(t)$ unveil crucial insights on the underlying mechanism for such a transition. The snapshots of $\kappa_{ij}^{AB}(t)$ are plotted in Figs. 2(a)–2(d) for $\Lambda_\varepsilon = -0.5$. It is evident that a single large frequency cluster emerges at the interface of the populations [Fig. 2(a)] due to strong interpopulation adaptation ($\varepsilon_{AB} > \varepsilon_{AA}$). As the oscillators in each population are arranged in the order of increasing frequencies, oscillators with nearby frequencies are entrained to form smaller intrapopulation clusters as in Fig. 2(a) for $\sigma = 0.7$. The interpopulation cluster grows in size with an increase in the coupling strength due to the subsequent entrainment of nearby oscillators [Figs. 2(a)–2(c)], which leads to gradual increase in the synchronization index S as in Fig. 1 and eventually results in the multistep transition to global synchronization [Fig. 2(d)]. Note that the strong interpopulation adaptation facilitates the rapid entrainment of oscillators from different populations resulting in the intercluster nucleation, which in turn leads to the multistep transition. In contrast, the intercluster nucleation is seeded by the disorder at $\langle \omega \rangle = 0$ in [32]. In stark contrast, for $\Lambda_\varepsilon > 0$, the network exhibits a single-

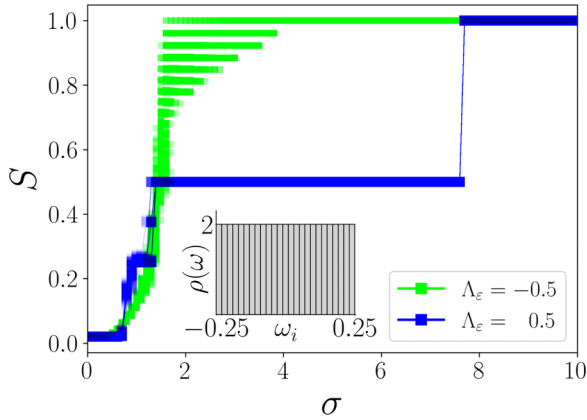


FIG. 1. Synchronization transition of the system of $N = 50$ globally coupled phase oscillators (1) for 500 realizations. The coupling strength disparity is fixed as $\Lambda_\sigma = 0$. The system undergoes a multistep transition for $\Lambda_\varepsilon = -0.5$, whereas for $\Lambda_\varepsilon = 0.5$ system follows a single-step transition to synchrony. The inset illustrates that the natural frequencies of the oscillators are drawn from a uniform distribution in the range of $[-0.25, 0.25]$. We have fixed $\delta = 0.001$. Other parameters are $\beta = -0.53\pi$ and $\varepsilon = 0.01$.

step transition to global synchronization as corroborated by S in Fig. 1 for $\Lambda_\varepsilon = 0.5$ (blue/dark gray squares). Again, $\kappa_{ij}^{AB}(t)$ uncover the underlying mechanism for such an abrupt synchronization transition. The snapshots of $\kappa_{ij}^{AB}(t)$ for $\Lambda_\varepsilon = 0.5$ are depicted in Figs. 2(e)–2(h). Strong intrapopulation adaptation ($\varepsilon_{AA} > \varepsilon_{AB}$) for $\Lambda_\varepsilon > 0$ facilitates intrapopulation clusters [Fig. 2(e)] due to rapid entrainment of nearby oscillators within populations. The intrapopulation clusters enlarge [Fig. 2(f)] and eventually manifest as completely entrained intrapopulation clusters as a function of the coupling strength [Fig. 2(g)], which results in gradual increase in the synchronization index $S \approx 0.5$ as in Fig. 1. Finally, the completely entrained intrapopulation clusters coalesce together above a critical coupling strength resulting in single-step transition to global synchronization [Fig. 2(h)], which is corroborated by

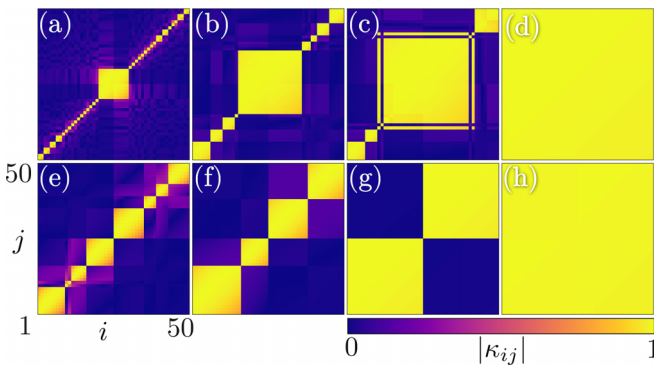


FIG. 2. The evolution of coupling weights with coupling strength σ in the absence of the coupling strength disparity $\Lambda_\sigma = 0$ elucidating multistep transition facilitated by interpopulation frequency cluster (a)–(d) for $\Lambda_\varepsilon = -0.5$, and single-step transition facilitated by intrapopulation frequency clusters (e)–(h) for $\Lambda_\varepsilon = 0.5$. The values of σ are (a) 0.7, (b) 1.2, (c) 1.4, (d) 3.9, (e) 0.75, (f) 0.95, (g) 5.0, and (h) 7.7. Other parameters are the same as in Fig. 1.

an abrupt jump in the synchronization index to $S = 1$ (Fig. 1 for $\Lambda_\varepsilon = 0.5$). Note that the strong intrapopulation adaptation facilitates the rapid entrainment of oscillators from within populations resulting in the intracluster nucleation, which in turn leads to the single-step transition. In contrast, the intracluster nucleation is seeded by the disorders symmetrically located away from $\langle \omega \rangle = 0$ in [32]. Thus, one can reinforce a particular route to the phase transition by tuning the time scale of adaptation.

Heat maps of S are depicted in the $(\sigma, \Lambda_\varepsilon)$ parameter space in Figs. 3(a)–3(c) for three distinct Λ_σ . For $\Lambda_\sigma = 0$, there is a single-step transition for $\Lambda_\varepsilon > 0$ and multistep transition for $\Lambda_\varepsilon < 0$ [Fig. 3(a)] as discussed above. Nevertheless, the effect of tradeoff between Λ_σ and Λ_ε is evident from Figs. 3(b) and 3(c) obtained for $\Lambda_\sigma = -0.5$ and 0.5 , respectively. Stronger interpopulation coupling strength (σ_{AB}) for $\Lambda_\sigma = -0.5$ and stronger interpopulation adaptation (ε_{AB}) in the range of $\Lambda_\varepsilon \in [-1, 0)$ manifest multistep transitions [Fig. 3(b)]. Despite strong intrapopulation adaptation (ε_{AA}), the stronger intrapopulation coupling (σ_{AA}) facilitates multistep transition in the range of $\Lambda_\varepsilon \in (0, 0.7)$ in Fig. 3(b). This elucidates that the coupling disparity (Λ_σ) dominates the adaptation disparity (Λ_ε) in facilitating phase transitions. However, when $\Lambda_\varepsilon \rightarrow 1$, $\varepsilon_{AB} \rightarrow 0$, and hence stronger ε_{AA} facilitates nucleation of clusters within populations which results in entrained intrapopulations and eventually facilitating a single-step transition despite a stronger σ_{AB} in the range of $\Lambda_\varepsilon \in (0.7, 0.9)$. Further, $\varepsilon_{AB} \approx 0$ when $\Lambda_\varepsilon \approx 1$ and consequently only two-cluster state manifest without any global synchronization. Both $\varepsilon_{AA} > \varepsilon_{AB}$ and $\sigma_{AA} > \sigma_{AB}$ facilitate nucleation within intrapopulations and a single-step transition in the range of $\Lambda_\varepsilon \in (0, 1)$ in Fig. 3(c) for $\Lambda_\sigma = 0.5$. Now, again a stronger σ_{AA} leads to a single-step transition even in the range of $\Lambda_\varepsilon \in (0, -0.5)$ [Fig. 3(c)], where interpopulation adaptation is larger, which reinforces that the coupling disparity (Λ_σ) dominates the adaptation disparity. However, $\varepsilon_{AB} \gg \varepsilon_{AA}$ for $\Lambda_\varepsilon \in (-0.5, -1)$ and hence a single large nucleation manifests at the population interface leading to a multistep transition.

Mesoscopic dynamics. Being evident that the transition from asynchrony to global synchronization involves nucleation and merging of frequency clusters, the dynamics of the full system can be captured by cluster level description. In the following, we employ a collective coordinate approach to analyze the synchronization of intrapopulation clusters [32,47,51,52]. First, we will sketch out the derivation of the cluster level approximation and show that it captures the synchronization transitions of the full system (1). Then, we will use a perturbation approach in the weak coupling limit to estimate the coupling strength at which the single-step transition takes place. The dynamical variables corresponding to the phase and coupling weights of an oscillator can be expressed in terms of collective coordinates $\phi_{i,\mu}^\eta(t)$ and $\kappa_{\mu\nu}^{\eta\eta'}(t)$ with the ansatz

$$\phi_i^\eta \approx \phi_{i,\mu}^\eta = \Theta_\mu^\eta(t)(\omega_i^\eta - \Omega_\mu^\eta) + f_\mu^\eta(t), \quad (4a)$$

$$\kappa_{ij}^{\eta\eta'}(t) \approx \kappa_{\mu\nu}^{\eta\eta'}(t). \quad (4b)$$

We consider N_c^η number of clusters in the η th population, and clusters are described by indices μ, ν . The term

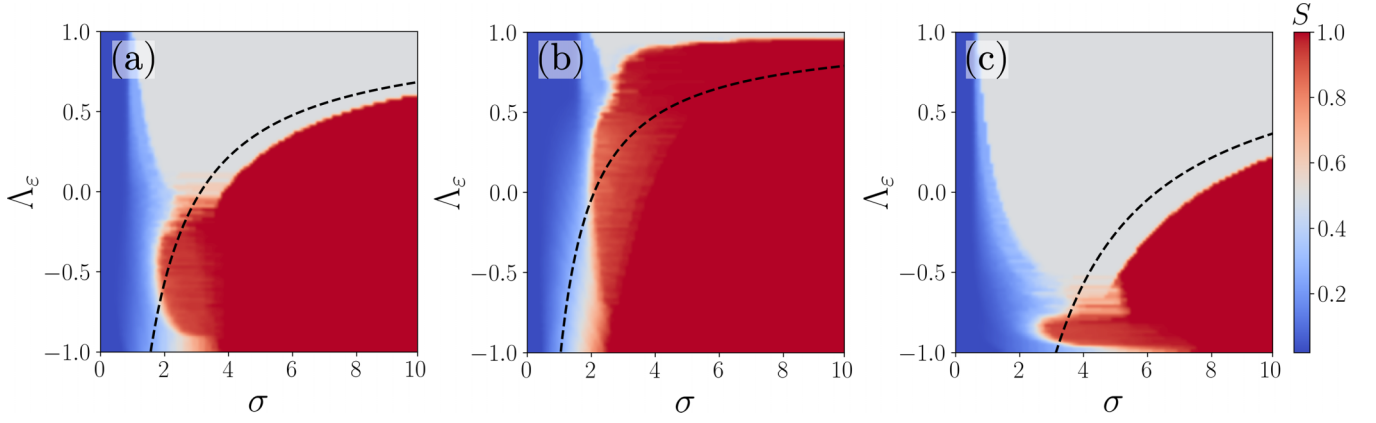


FIG. 3. Heat maps of synchronization index S , for ten different realizations, in the $(\sigma, \Lambda_\varepsilon)$ parameter space elucidating multistep and single-step transitions. (a) $\Lambda_\sigma = 0$, (b) $\Lambda_\sigma = -0.5$, and (c) $\Lambda_\sigma = 0.5$. The dashed black curve is the analytical estimate for the upper bound for the two cluster state. Other parameters are the same as in Fig. 1.

$\Theta_\mu^\eta(\omega_i^\eta - \Omega_\mu^\eta)$ describes the frequency drift of the i th oscillator within the μ th cluster in the population η , Ω_μ^η and f_μ^η are the mean frequency and collective phase of the μ th cluster, respectively. $\kappa_{\mu\nu}^{\eta\eta'}$ governs the intercluster coupling weights. Errors arising in describing the evolution of the phase and coupling weights in terms of collective coordinates can be defined as $E_{\phi_i^\eta} = \dot{\phi}_{i,\mu}^\eta - \dot{\phi}_i^\eta$ and $E_{\kappa_{ij}^{\eta\eta'}} = \dot{\kappa}_{\mu\nu}^{\eta\eta'} - \dot{\kappa}_{ij}^{\eta\eta'}$, respectively. The evolution equations for the collective coordinates $(\Theta_\mu^\eta, f_\mu^\eta, \kappa_{\mu\nu}^{\eta\eta'})$ are obtained by requiring the error $\mathbf{E} = (E_{\phi_1^\eta}, \dots, E_{\phi_{N_\eta}^\eta}, E_{\phi_1^{\eta'}}, \dots, E_{\phi_{N_{\eta'}}^{\eta'}}, \dots, E_{\kappa_{11}^{\eta\eta}}, \dots, E_{\kappa_{N_\eta N_\eta}^{\eta\eta}}, E_{\kappa_{11}^{\eta\eta'}}, \dots, E_{\kappa_{N_{\eta'} N_{\eta'}}^{\eta\eta'}})$ to be orthogonal to the manifold of the ansatz. The frequency distribution corresponding to the μ th cluster of the η th population can be expressed as $\rho_\mu^\eta(\omega) = 2/n_\mu^\eta$ for $(\Omega_\mu^\eta - 0.25n_\mu^\eta \leq \omega \leq \Omega_\mu^\eta + 0.25n_\mu^\eta)$, and zero otherwise. Here, n_μ^η is the ratio (N_μ^η/N) of oscillators. In the continuum limit, the cluster order parameter $r_\mu^\eta = 1/N_\mu^\eta |\sum_{i \in C_\mu} e^{i\phi_{i,\mu}^\eta}|$ can be expressed as $r_\mu^\eta = (4/n_\mu^\eta \Theta_\mu^\eta) \sin(n_\mu^\eta \Theta_\mu^\eta / 4)$ with the variance of natural frequencies of the cluster as $\xi_\mu^\eta = (n_\mu^\eta)^2 / 48$. Consequently, the evolution equations for the collective coordinates are governed by

$$\dot{\Theta}_\mu^\eta = 1 + \frac{1}{\xi_\mu^\eta \Theta_\mu^\eta} \left[\cos\left(\frac{n_\mu^\eta \Theta_\mu^\eta}{4}\right) - r_\mu^\eta \right] \times \left[\sum_{\eta'} \sum_{\nu} n_\nu^{\eta'} r_\nu^{\eta'} \sigma_{\eta\eta'} \kappa_{\mu\nu}^{\eta\eta'} \cos(f_\mu^\eta - f_\nu^{\eta'}) \right], \quad (5a)$$

$$\dot{f}_\mu^\eta = \Omega_\mu^\eta - r_\mu^\eta \sum_{\eta'} \sum_{\nu} n_\nu^{\eta'} r_\nu^{\eta'} \sigma_{\eta\eta'} \kappa_{\mu\nu}^{\eta\eta'} \sin(f_\mu^\eta - f_\nu^{\eta'}), \quad (5b)$$

$$\dot{\kappa}_{\mu\nu}^{\eta\eta'} = -\varepsilon_{\eta\eta'} [\kappa_{\mu\nu}^{\eta\eta'} + r_\mu^\eta r_\nu^{\eta'} \sin(f_\mu^\eta - f_\nu^{\eta'} + \beta)]. \quad (5c)$$

In the context of the mesoscopic description, the synchronization index (2) can be redefined, to characterize the synchronization of frequency clusters, as

$$S = \sum_{\eta, \eta'} \sum_{\mu, \nu} n_\mu^\eta n_\nu^{\eta'} s_{\mu\nu}^{\eta\eta'}. \quad (6)$$

Akin to microscopic context (3), $s_{\mu\nu}^{\eta\eta'} = 1$, if $\langle \dot{f}_\mu^\eta \rangle = \langle \dot{f}_\nu^{\eta'} \rangle$, otherwise $s_{\mu\nu}^{\eta\eta'} = 0$. Although the single-step transition can be described by a minimum of two clusters, a larger number of clusters are required for a complete description of the multistep transition. The phase transitions displayed by S (6), estimated from the evolution equations for the collective coordinates, corresponding to two populations of four clusters each are depicted in Fig. 4 for two values of Λ_ε . It is evident from the figure that the collective coordinate approach clearly displays single-step and multistep transitions for $\Lambda_\varepsilon = 0.5$ and -0.5 , respectively, in agreement with the simulation results in Fig. 1.

Now, an analytical estimate of the upper bound for the coupling strength corresponding to the completely entrained clusters of intrapopulations [Fig. 2(g)] during the single-step transition can be obtained using the perturbative approach in the weak coupling limit [32]. Assuming the intracluster phase difference ($f = f_\mu - f_\nu$) grows linearly in time with

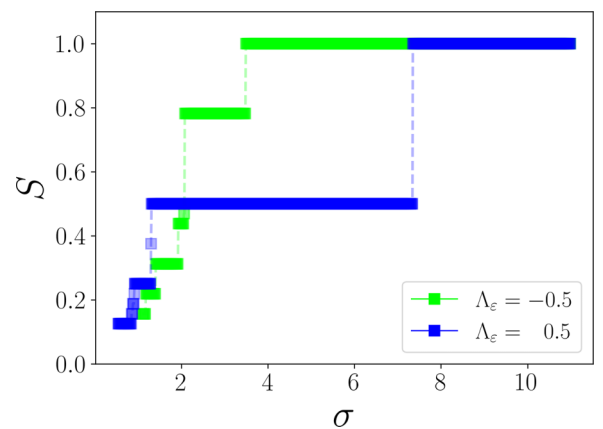


FIG. 4. Phase transitions from the evolution equations for the collective coordinates corresponding to two populations each having four clusters for $\Lambda_\sigma = 0$ corroborating the simulation results in Fig. 1. The natural angular frequencies of clusters (Ω_μ^η) are drawn from uniform frequency distribution in the range $[-0.25, 0.25]$. Other parameters are the same as in Fig. 1.

the relative phase velocity Ω' , the collective coordinates can be expressed in terms of perturbation in α as

$$\Theta_\mu(t) = \Theta_\mu^{(0)} + \alpha\Theta_\mu^{(1)}(t) + \mathcal{O}(\alpha^2), \quad (7a)$$

$$\kappa_{\mu\nu}(t) = \kappa_{\mu\nu}^{(0)} + \alpha\kappa_{\mu\nu}^{(1)}(t) + \mathcal{O}(\alpha^2), \quad (7b)$$

$$f(t) = \Omega't + \alpha f^{(1)}(t) + \mathcal{O}(\alpha^2). \quad (7c)$$

Substituting the perturbed equations in (5) leads to the quadratic equation in Ω'

$$(\Omega')^2 + \Omega'(\Omega_\mu - \Omega_\nu) - \frac{\varepsilon_{\mu\nu}\sigma_{\mu\nu}}{2}(r_\mu^{(0)}r_\nu^{(0)})^2 \sin\beta = 0. \quad (8)$$

The condition for the existence of the real solution of (8) requires $(\Omega_\mu - \Omega_\nu)^2 \geq -2\varepsilon_{\mu\nu}\sigma_{\mu\nu}(r_\mu^{(0)}r_\nu^{(0)})^2 \sin\beta$. Now, the upper bound for the coupling strength for the existence of the completely entrained intrapopulation clusters can be obtained as

$$\sigma_c = \left(\frac{(\Omega_\mu - \Omega_\nu)^2}{2\varepsilon(1 - \Lambda_\varepsilon)(1 - \Lambda_\sigma)(r_\mu^{(0)}r_\nu^{(0)})^2 \sin(-\beta)} \right). \quad (9)$$

It is evident that σ_c depends explicitly on the adaptation and the coupling strength disparities. For a rough estimate of σ_c , one can consider $r_\mu^{(0)} \approx r_\nu^{(0)} \approx 1$. For the values of the parameters in Fig. 1, the upper bound can be obtained as $\sigma_c = 6.28$ with $\Omega_\mu - \Omega_\nu = -0.25$, which almost agrees with the single-step transition in Figs. 1 and 4. Now, the critical curve corresponding to the upper bound can be obtained as $\Lambda_\varepsilon = 1 - [(\Omega_\mu - \Omega_\nu)^2 / (2\varepsilon\sigma_c(1 - \Lambda_\sigma)(r_\mu^{(0)}r_\nu^{(0)})^2 \sin(-\beta))]$, which is depicted as a dashed curve in Figs. 3(a)–3(c) across which the single-step transition takes place. The finite size effect and the first order approximation for the order parameters $r_\mu^{(0)}$ and $r_\nu^{(0)}$ contribute to the error between the analytical estimate and the numerical results in Fig. 3.

Discussion and conclusion. We have considered a globally coupled finite-size adaptive network, wherein the subpopulations are distinguished by different degrees of time scale adaptation (Λ_ε) and coupling strength (Λ_σ) but with uniform distribution of natural frequencies. We have found that nucleations of intrapopulation frequency clusters coalesce at the interface of the two populations facilitating the manifestation of a single large interpopulation frequency cluster for a strong interpopulation adaptation rate, $\Lambda_\varepsilon < 0$, without any coupling strength disparity. Eventually, the single large interfrequency cluster grows to the system size as the coupling strength is increased, facilitating a multistep transition to global synchronization. In contrast, nucleations of intrapopulation frequency clusters coalesce among themselves to manifest completely entrained two intrapopulation frequency clusters as a function of the coupling strength for a strong intrapopulation adaptation rate $\Lambda_\varepsilon > 0$, without any coupling strength disparity. Finally, the two intra-frequency-clusters coalesce together facilitating a single-step transition to global synchronization.

Synchronization index S clearly displays the two distinct transitions for two distinct values of Λ_ε when $\Lambda_\sigma = 0$.

Further, we found that a strong interpopulation coupling strength, $\Lambda_\sigma < 0$, always favors nucleation of interfrequency clusters leading to multistep transition even for a strong intrapopulation adaptation rate ($\Lambda_\varepsilon > 0$). Furthermore, we found that a strong intrapopulation coupling strength, $\Lambda_\sigma > 0$, always favors nucleation of intrafrequency clusters facilitating single-step transition even with a strong interpopulation adaptation rate ($\Lambda_\varepsilon < 0$). These results corroborate that the degree of disparity in the coupling strength strongly determines the nature of nucleation leading to distinct synchronization transition. We have analytically deduced the macroscopic evolution equations for the cluster dynamics using the framework of collective coordinates [47]. The synchronization transitions obtained using the collective coordinates are found to agree with the simulation results. Further, we have also deduced the upper bound for the coupling strength for the existence of two intraclusters explicitly in terms of adaptation and coupling strength disparity parameters, which is found to almost match the coupling strength at the onset of abrupt single-step transition. It is also evident that the mesoscopic description brilliantly captures the multicenter dynamics.

Note that similar heterogeneous nucleation resulting in multi- and single-step transitions are reported to be facilitated by distinct quenched disorders [32], wherein the nucleations emerge at the site of the disorder(s) resulting in multi-(single-)step transitions. However, in our case with uniform distribution of natural frequencies, small intracluster nucleations coalesce either at the population interface or within the populations resulting in multi- and single-step synchronization transitions depending on the trade off between the adaptation and coupling disparities. Understanding the mechanism of nucleations corresponding to distinct transition due to the inherent disparities of complex real-world systems is of paramount importance as they shed more light on the role of disparities among different regions of the brain in synchronization in unraveling brain functions and neurological disorders [53], segregation and polarization dynamics in social networks [46], etc. Moreover, our findings hold significance in the network control theory, offering strategies to optimize adaptive networks.

Acknowledgments. We thank the anonymous referees for their insightful comments that have greatly improved the presentation of the manuscript. We also thank Ola Ali from the Complexity Science Hub for her comments. A.K. acknowledges the financial support from IISER-TVM. J.F. acknowledges funding by the Austrian Science Fund (FWF): I 5985-N. The work of V.K.C. is supported by the DST-CRG Project under Grant No. CRG/2020/004353 and V.K.C. wishes to thank DST, New Delhi for computational facilities under the DST-FIST programme (SR/FST/PS- 1/2020/135) to the Department of Physics. DVS is supported by the DST-SERB-CRG Project under Grant No. CRG/2021/000816.

[1] S. Boccaletti, V. Latora, Y. Moreno, M. Chavez, and D.-U. Hwang, *Phys. Rep.* **424**, 175 (2006).

[2] S. H. Strogatz, *Nature (London)* **410**, 268 (2001).

[3] M. E. J. Newman, *SIAM Rev.* **45**, 167 (2003).

- [4] S. Boccaletti, A. N. Pisarchik, C. I. Del Genio, and A. Amann, *Synchronization: From Coupled Systems to Complex Networks* (Cambridge University Press, Cambridge, England, 2018).
- [5] F. Dörfler, M. Chertkov, and F. Bullo, *Proc. Natl. Acad. Sci. USA* **110**, 2005 (2013).
- [6] S. Shahal, A. Wurzberg, I. Sibony, H. Duadi, E. Shniderman, D. Weymouth, N. Davidson, and M. Fridman, *Nat. Commun.* **11**, 3854 (2020).
- [7] D. Bagchi and P. K. Mohanty, *Phys. Rev. E* **84**, 061921 (2011).
- [8] M. Conover, J. Ratkiewicz, M. Francisco, B. Goncalves, F. Menczer, and A. Flammini, *Proceedings of the International AAAI Conference on Web and Social Media* **5**, 89 (2021).
- [9] M. Levy, *J. Econ. Dyn. Control* **32**, 137 (2008).
- [10] A. Arenas, A. Díaz-Guilera, J. Kurths, Y. Moreno, and C. Zhou, *Phys. Rep.* **469**, 93 (2008).
- [11] J. Gómez-Gardeñes, Y. Moreno, and A. Arenas, *Phys. Rev. Lett.* **98**, 034101 (2007).
- [12] S. Dutta, P. Kundu, P. Khanra, C. Hens, and P. Pal, *Phys. Rev. E* **108**, 024304 (2023).
- [13] W. Gerstner, R. Kempter, J. L. Van Hemmen, and H. Wagner, *Nature (London)* **383**, 76 (1996).
- [14] N. Caporale and Y. Dan, *Annu. Rev. Neurosci.* **31**, 25 (2008).
- [15] V. Röhr, R. Berner, E. L. Lameu, O. V. Popovych, and S. Yanchuk, *PLoS One* **14**, e0225094 (2019).
- [16] M. M. Waldrop, *Nature (London)* **503**, 22 (2013).
- [17] G. B. Morales, C. R. Mirasso, and M. C. Soriano, *Neurocomputing* **461**, 705 (2021).
- [18] R. Berner, S. Yanchuk, and E. Schöll, *Phys. Rev. E* **103**, 042315 (2021).
- [19] S. R. Proulx, D. E. Promislow, and P. C. Phillips, *Trends in Ecology & Evolution* **20**, 345 (2005).
- [20] T. Gross, C. J. D. D’Lima, and B. Blasius, *Phys. Rev. Lett.* **96**, 208701 (2006).
- [21] I. Rajapakse, M. Groudine, and M. Mesbahi, *Proc. Natl. Acad. Sci. USA* **108**, 17257 (2011).
- [22] L. Horstmeyer and C. Kuehn, *Phys. Rev. E* **101**, 022305 (2020).
- [23] F. Baumann, P. Lorenz-Spreen, I. M. Sokolov, and M. Starnini, *Phys. Rev. Lett.* **124**, 048301 (2020).
- [24] D. Antoniadou and C. Drovolis, *Comput. Social Networks* **2**, 14 (2015).
- [25] J. Sawicki, R. Berner, S. A. M. Loos, M. Anvari, R. Bader, W. Barfuss, N. Botta, N. Brede, I. Franović, D. J. Gauthier *et al.*, *Chaos* **33**, 071501 (2023).
- [26] B. Jüttner and E. A. Martens, *Chaos* **33**, 053106 (2023).
- [27] R. Berner, *Patterns of Synchrony in Complex Networks of Adaptively Coupled Oscillators*, Springer Theses (Springer, Cham, Switzerland, 2021).
- [28] R. Berner, E. Schöll, and S. Yanchuk, *SIAM J. Appl. Dyn. Syst.* **18**, 2227 (2019).
- [29] S. Thamizharasan, V. K. Chandrasekar, M. Senthilvelan, R. Berner, E. Schöll, and D. V. Senthilkumar, *Phys. Rev. E* **105**, 034312 (2022).
- [30] R. Berner, A. Polanska, E. Schöll, and S. Yanchuk, *Eur. Phys. J.: Spec. Top.* **229**, 2183 (2020).
- [31] M. Thiele, R. Berner, P. A. Tass, E. Schöll, and S. Yanchuk, *Chaos* **33**, 023123 (2023).
- [32] J. Fialkowski, S. Yanchuk, I. M. Sokolov, E. Schöll, G. A. Gottwald, and R. Berner, *Phys. Rev. Lett.* **130**, 067402 (2023).
- [33] R. Berner, T. Gross, C. Kuehn, J. Kurths, and S. Yanchuk, *Phys. Rep.* **1031**, 1 (2023).
- [34] M. Girvan and M. E. Newman, *Proc. Natl. Acad. Sci. USA* **99**, 7821 (2002).
- [35] M. E. Newman, *Proc. Natl. Acad. Sci. USA* **103**, 8577 (2006).
- [36] P. J. Mucha, T. Richardson, K. Macon, M. A. Porter, and J.-P. Onnela, *Science* **328**, 876 (2010).
- [37] R. F. Betzel and D. S. Bassett, *NeuroImage* **160**, 73 (2017).
- [38] R. B. Garabed, A. Jolles, W. Garira, C. Lanzas, J. Gutierrez, and G. Rempala, *Interface Focus* **10**, 20190118 (2020).
- [39] D. Brockmann and D. Helbing, *Science* **342**, 1337 (2013).
- [40] G. Quaranta, G. Formica, J. T. Machado, W. Lacarbonara, and S. F. Masri, *Nonlinear Dyn.* **101**, 1583 (2020).
- [41] J. C. Flack, *Phil. Trans. R. Soc. B* **367**, 1802 (2012).
- [42] J. Saramäki and E. Moro, *Eur. Phys. J. B* **88**, 164 (2015).
- [43] C. Guo, J. Wang, J. Li, Z. Wang, and S. Tang, *J. Phys. Chem. Lett.* **7**, 5008 (2016).
- [44] S. Xu, D. Cao, Y. Liu, and Y. Wang, *Cryst. Growth Des.* **22**, 2001 (2022).
- [45] T. Evans and F. Fu, *R. Soc. Open Sci.* **5**, 181122 (2018).
- [46] G. Tóth, J. Wachs, R. Di Clemente, Á. Jakobi, B. Ságvári, J. Kertész, and B. Lengyel, *Nat. Commun.* **12**, 1143 (2021).
- [47] G. A. Gottwald, *Chaos* **25**, 053111 (2015).
- [48] J. A. Acebrón, L. L. Bonilla, C. J. Pérez Vicente, F. Ritort, and R. Spigler, *Rev. Mod. Phys.* **77**, 137 (2005).
- [49] T. Aoki and T. Aoyagi, *Phys. Rev. Lett.* **102**, 034101 (2009).
- [50] T. Aoki and T. Aoyagi, *Phys. Rev. E* **84**, 066109 (2011).
- [51] E. J. Hancock and G. A. Gottwald, *Phys. Rev. E* **98**, 012307 (2018).
- [52] L. D. Smith and G. A. Gottwald, *Chaos* **30**, 093107 (2020).
- [53] C. J. Stam, *Nat. Rev. Neurosci.* **15**, 683 (2014).